

Final Technical Report
NEHRP/USGS Award Number: G09AP00114

**Title: Systematic Analysis of Early Aftershocks of the 2004 Mw6.0 Parkfield Earthquake
Detected by a Matched Filter Technique**

Principal Investigator: Zhigang Peng
School of Earth and Atmospheric Sciences
Georgia Institute of Technology
311 Ferst Drive
Atlanta, GA 30332
TEL: 404-894-0231
FAX: 404-894-5638
EMAIL: zpeng@gatech.edu

Term covered by this award: July 1, 2009 – June 30, 2010

Submitted: September 29, 2010

Abstract

Large shallow earthquakes are typically followed by increased seismic activity, known as “aftershocks”, which diminish in rate approximately as the inverse of the elapsed time since the mainshock. Although aftershocks have been observed for more than one century, the underlying physics of aftershock generation and earthquake triggering remains in debate (e.g., Felzer and Brodsky, 2006; Richards-Dinger et al., 2010). An important discrimination of various triggering models is in the very early stage of the aftershock sequences, when the seismicity rate is extremely high. However, many aftershocks are likely missing in the existing catalogs immediately after the mainshock. A robust and rapid detection of these missing early aftershocks would not only improve our understanding of earthquake triggering and the underlying physical mechanism, but also provide crucial information about the mainshock rupture area and directivity effect. Such information is important for assessing the quality, completeness, accuracy and magnitude completeness of earthquake catalogs, and is critical for rapid assessment of the damage and societal impact generated by large earthquakes.

We have conducted a systematic search of missing early aftershocks along the Parkfield section of the San Andreas Fault (SAF) after the 2004 Mw6.0 Parkfield earthquake (Peng and Zhao, 2009). By using 2-8 Hz band-pass-filtered waveforms recorded by the borehole High Resolution Seismic Network (HRSN) and generated by ~3600 events as templates, we have identified 11 times more aftershocks than reported in the standard Northern California Seismic Network (NCSN) catalog in the first three days after the 2004 Parkfield mainshock. The nearly 10-fold increase of events immediately after the Parkfield mainshock show clear migrations in both along-strike and down-dip directions with logarithmic time since the mainshock, which is compatible with the models of afterslip driving aftershocks (Kato, 2007) or the Dieterich (1994) rate-state friction.

In the second study (Meng et al., 2010), we focused on the time periods immediately before and after the 2003 Mw6.5 San Simeon earthquake. The San Simeon mainshock has produced a positive Coulomb stress changes on the Parkfield section of the SAF, and triggered right-lateral surface creep on the SAF observed by the USGS creepmeters. However, the seismicity rate calculated from the NCSN catalog does not show any observable changes caused by the San Simeon earthquake. Using the same templates around Parkfield, we found a total of 277 events 48 hours before and 30 hours after 2003 San Simeon earthquake, of which only 7 are listed in the NCSN catalog. The seismicity rate from the newly detected events shows a clear increase around Parkfield during the San Simeon mainshock. In comparison, swarm-like activity south of Gold Hill started about 2 days before and turned off immediately before the mainshock, which resulted in a decrease of seismicity rate. No detections are found further north in the creeping section of the SAF either before or after the mainshock. Our observations suggest that the SAF near Parkfield was positively loaded by the San Simeon earthquake. This is consistent with the Coulomb stress calculation and triggered creep observations, although we cannot rule out the possibility of dynamic triggering.

Our results suggest that the matched filter technique is effective in detecting missing events immediately after nearby large earthquakes in Central California. Our ongoing work is to apply the same technique to detect missing events in Southern California (Doran et al., 2010) and Japan (Enescu et al., 2010), and use the newly identified events to better quantify the underlying physical mechanism of earthquake triggering.

Main body of the text

1. Significance of the project

The research objective of this project is to systematically detect aftershocks (triggered seismicity) around the Parkfield section of the SAF (Figure 1) immediately after moderate earthquakes in Central California. The time period immediately after the mainshock holds valuable information on the transition from mainshock to aftershocks, and the underlying earthquake physics that controls the time-dependent behavior of aftershocks. A systematic detection and analysis of the early aftershocks would provide a new insight into the mainshock rupture processes and the early post-seismic relaxation processes around the Parkfield region. A direct comparison of the temporal evolution of aftershocks and afterslip in the early stage of the postseismic relaxation processes can greatly advance our understanding of the physical mechanism of aftershock generation, and provide important clues on the frictional properties of San Andreas fault (SAF) around Parkfield. This in turn, will result in improved knowledge on what controls the variability of fault slip behaviors (e.g., continuous creep, episodic slip events, afterslip, microearthquakes, large earthquake ruptures).

One of the USGS/EHP's long-term goals is to mitigate earthquake losses in the US by focusing on observations, theory, experiments, and developing testable models of earthquake and tectonic processes and of earthquake effects. Our proposed work would directly contribute to the USGS's long-term efforts at Parkfield on understanding earthquake phenomena and evaluating earthquake hazards through the Parkfield Earthquake Prediction Experiment and the recent San Andreas Fault Observatory at Depth (SAFOD) project.

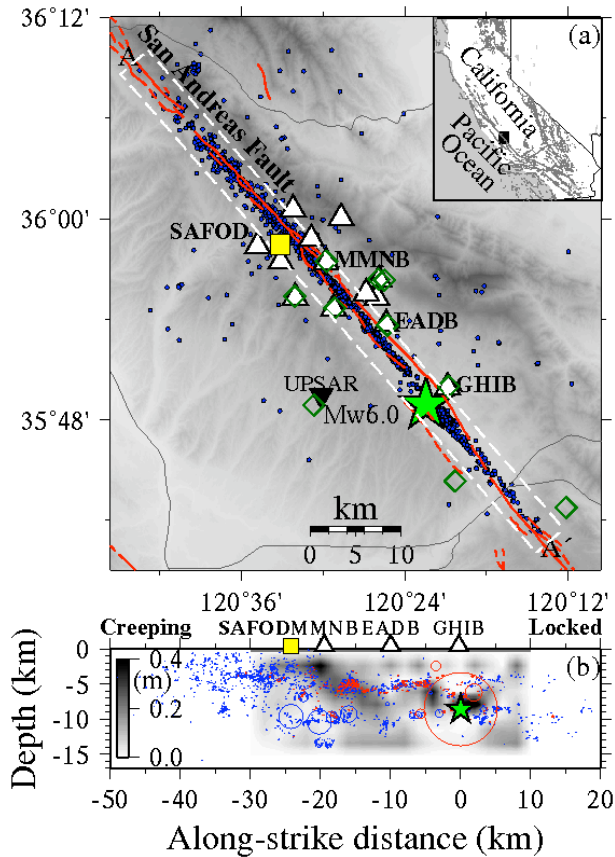


Figure 1. (a) Map of the Parkfield section of the San Andreas fault (SAF). The inset illustrates the tectonic environment in California. (b) The cross-section view of the 3647 template events along the SAF. The red symbol denotes locations of the detected events within the first hour after the Parkfield mainshock by Peng and Zhao (2009).

2. Matched Filter Detection of the Parkfield Early Aftershock

2.1 The 2004 Mw6.0 Parkfield earthquake sequences and the data set

The Parkfield section of the SAF (Figure 1) straddles the transition between the creeping segment of the fault to the northwest and the locked segment to the southeast that last broke in the great 1857 Fort Tejon earthquake (Sieh, 1978). At least 7 characteristic earthquakes of ~M6 occurred at Parkfield since 1857, with the most recent on September 28th 2004 (Bakun et al., 2005). The quasi-periodicity of the previous 6 events led to the deployment of many seismic and

other instruments as part of the Parkfield Earthquake Prediction Experiment (Bakun and Lindh, 1985). The instrumentation was further augmented with the recent development of the San Andreas Fault Observatory at Depth (SAFOD) project (Hickman et al., 2004). The 2004 Mw6.0 Parkfield earthquake nucleated near Gold Hill, and the rupture propagated predominately in the NW direction with a total length of ~ 30 km (Bakun et al., 2005). Many near-field, unclipped, and continuous seismograms for the mainshock and its aftershocks were recorded, resulting in one of the best recorded earthquake sequences in the world (Harris and Arrowsmith, 2006).

In both studies as describe below (Peng and Zhao, 2009; Meng et al., 2010), we used seismic data recorded by the High Resolution Seismic Network (HRSN) operated by UC Berkeley. The HRSN has 13 borehole short-period instruments that recorded waveforms continuously since 2001. In addition, the entire seismicity in Parkfield from 1984 and 2005, including aftershocks of the 2004 Parkfield earthquake, have been relocated using a double-difference technique and 3D velocity model (Thurber et al., 2006). The goal is to use those events listed in the Thurber et al. (2006) catalog and recorded by the HRSN as the matched filter to detect missing events around the Parkfield section of the SAF after the 2003 Mw6.5 San Simeon and 2004 Mw6.0 Parkfield earthquakes.

2.2 Analysis Procedure

The analysis procedure generally follows that of Shelly et al. (2007a, 2007b) and is briefly described here. The seismic data is recorded by the 13 3-component short-period borehole stations of the High Resolution Seismic Network (HRSN) operated by UC Berkeley. We use 3-component seismograms recorded by the BP channel (20 samples/s) of the HRSN as templates, and search through 3-day continuous recordings since 2004/09/28 to detect seismic events by waveform cross-correlation. A two-way 4th order 2-8 Hz Butterworth filter is applied to both the template and continuous waveforms. Next, we compute the P and S wave arrival times for each event using a 1-D velocity model in this region (Waldhauser et al., 2004) with a nominal V_p/V_s ratio of 1.732. A 4-s time window starting 2 s before the computed S -wave arrivals is used as the waveform template window (signal). The noise level is obtained from a 4-s time window 6 s before the computed P -wave arrivals. We require that each template event is recorded by at least 4 out of the 13 stations (12 channels) with a minimum signal-to-noise ratio (SNR) of 5. In addition, each template event needs to have a magnitude that can be used to calibrate the magnitude of the detected event. After the section process, we obtain a total of 3647 earthquakes listed in the Thurber et al. (2006) relocated catalog as our template events.

We shift the 4-s time window around the computed S arrival in an increment of 0.05 s (1 sample) through the 3-day continuous waveforms. At each time point, we compute the correlation coefficient (CC), and assign the CC value to its origin time by subtracting the computed S -wave arrival time. Next, we stack the CC values for all stations and components, and compute the mean CC value at each time point, which is used as a measure of similarity between the template and detected events. We compute the median absolute deviation (MAD) of the mean CC trace for each template event and use 9 times of MAD as the detection threshold (Shelly et al., 2007a). For a normally distributed random variable, the standard deviation σ is $1.4826 \times MAD$. The corresponding probability of exceedance for 9 times the MAD , or 5.4 times the σ , is 6.4×10^{-10} . In a 1-day period, we sample 172800 time steps for each template event. So the chance of random detection using the threshold of $9 \times MAD$ is about 1 event per day, suggesting that most of the detections correspond to real events, instead of false detection by random chance.

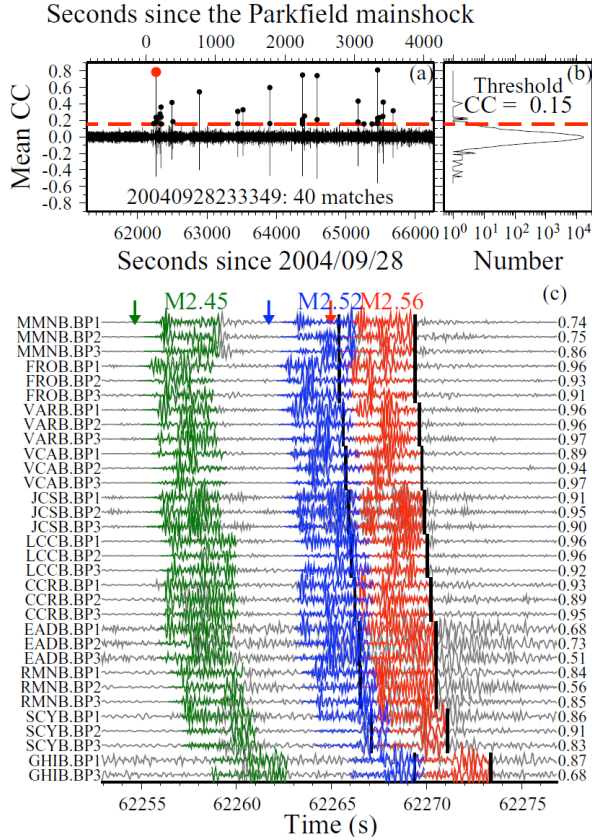


Figure 2. Example of an early aftershock detected at ~ 140 s after the Parkfield mainshock. (a) Mean cross-correlation (CC) functions for the template event 20040928233349. The black dots are positive detections above the threshold ($9 \times \text{MAD}$) and the red dot corresponds to the detected event (at 62264.95 s since 2004/09/28) with corresponding waveforms shown in (c). (b) The histogram of the mean CC functions. (c) A comparison of the template waveforms (red) and the continuous waveforms (gray). The station name and corresponding CC value are labeled on the left and right sides, respectively. The short black lines mark the start and end of the matched window. Waveforms shown in green and blue colors correspond to other two events that occurred nearby.

This is roughly consistent with the amplitude-magnitude relationship between the template and detected events listed in the Thurber et al. (2006) catalog. Overall, we have a total of 610286 positive detections between 09/28/2004 and 09/30/2004. After removing multiple detections, we obtain 11138 individual events. In comparison, only 543 and 933 events were listed in the Thurber et al. (2006) and the NCSN catalogs, respectively. Hence, our matched filter technique has detected at least 11 times more aftershocks than those in the NCSN catalog.

2.3 Space-time migration of the early aftershocks

Since the detected events have similar waveforms at multiple stations as compared to the template event, their hypocenter locations must be close or identical (Peng and Ben-Zion, 2006; Shelly et al., 2007a). For multiple detections in each 2-s window, we assign the location of template event with the highest mean CC value (Shelly et al., 2007a). Since some detected events are also listed in the Thurber et al. (2006) catalog, we compute the inter-hypocentral distance between the template events and these detected events listed in the catalog. We find that 95% of the events are within the distance of 2.7 km for CC values larger than 0.2, which roughly places an upper-limit of the location uncertainty of the detected events relative to the templates.

Figure 2 shows an example of a positive detection on 09/28/2004 17:17:44, approximately 140 s after the origin time of the mainshock (09/28/2004 17:15:24). The template event occurred on 09/28/2004 23:33:49 and has a duration magnitude $M_d = 2.47$. Based on the median amplitude ratio, we estimate that the detected event has a magnitude of 2.56. Although two additional events occurred within 10 s, the matched filter technique is able to uniquely identify the target event with a network-averaged CC value of 0.79. The waveforms of the other two events also match nearby templates. It is worth noting that none of these newly detected events (in the magnitude range of 2.4–2.6) are listed in the NCSN catalog.

Finally, we compute the magnitude of the detected event based on the median value of the maximum amplitude ratios for all channels between the template and detected events, assuming that a tenfold increase in amplitude corresponds to one unit increase in magnitude.

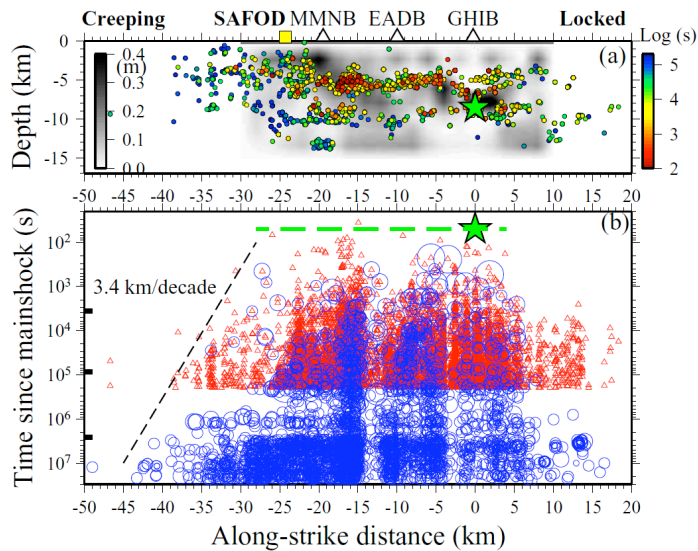


Figure 3. (a) The cross-section view of the all detected events along the SAF color-coded by the logarithmic time after the mainshock. The green star denotes the hypocenter of the mainshock. The background shading denotes the finite-fault slip distribution from Liu et al. (2006). (b) The occurrence times since the 2004 Parkfield mainshock versus the along-strike distances. The blue circles and the red triangles mark the events listed in the Thurber et al. (2006) catalog and detected by the matched filter technique, respectively. The black dashed line marks the approximate slope of aftershock migration along the creeping section of the SAF.

section of SAF. The migration speed is ~ 3.4 km per decade change in time since the mainshock. In comparison, the aftershocks SE of our study region appear to expand suddenly from 7 km to 17 km SE of the epicenter around 104 s (~ 3 hours) after the mainshock, rather than migrating with time as shown in the creeping section.

2.4 Comparison with other studies

It has been long recognized that aftershocks often migrate along the fault strike and down-dip directions (e.g., Chatelain et al., 1983; Tajima and Kanamori, 1985; Henry and Das, 2001). In some cases, aftershock zones show little expansion (Tajima and Kanamori, 1985), while in other cases, aftershock zones grow rapidly during the first few days following the mainshock, and the expansion slows down at later time (Chatelain et al., 1983). Such spatio-temporal migrations offer important clues on the physical mechanisms of aftershock generation. Dieterich (1994) proposed that the temporal decay and spatial expansion of aftershocks could be explained by a delayed response to the co-seismic stress changes for populations of faults around the mainshock rupture obeying the laboratory-derived rate-state friction law. Alternatively, recent observations of aftershocks and post-seismic deformation following an Omori-law-type decay with similar relaxation times have led to the suggestion that aftershocks are driven primarily by aseismic afterslip around the mainshock rupture zone (Perfettini et al., 2004; Hsu et al., 2006). Other possible mechanisms to trigger aftershocks include dynamic stress changes from passing seismic

Figure 3a shows the locations of the detected aftershocks color-coded by their occurrence time since the mainshock in logarithmic time scale. We find that most of the aftershocks within the first hour occur along a 12-km-long “streak” at the depth range of 4-6 km. In comparison, aftershocks in another seismic “streak” at the depth range of 8-10 km do not occur instantaneously and rigorously as those in the shallow “streak”. Finally, a cluster of deep events at 13 km below MM and the region north of the SAFOD in the creeping section were not active within the first few hours after the mainshock, indicating a possible migration of aftershocks along the SAF strike and the down-dip directions.

To investigate this further, we plot in Figure 4b the logarithmic occurrence time since the mainshock against the along-strike distance for all events within 2 km of the SAF. The newly detected events show clear migration with logarithmic time in the creeping

waves (Hill and Prejean, 2007), viscoelastic relaxation in the lower crust and upper mantle, or by fluid flows (Nur and Booker, 1972).

Many previous studies have found that postseismic deformation following the 2004 Parkfield earthquake mostly occurs as afterslip within the aseismic creeping patches of the SAF surrounding the locked asperity (Johnson et al., 2006; Langbein et al., 2006; Freed, 2007). The cumulative moment release from afterslip in 2 yrs after the mainshock is about 3 times the coseismic moment release (Barbot et al., 2009), suggesting that quasi-static stress changes from afterslip may play a more important role in triggering aftershocks than static stress changes from the Parkfield mainshock. In addition, the cumulative number of the Parkfield aftershocks and the postseismic deformation appear to be linearly related (Barbot et al., 2009; Savage and Langbein, 2008), and the cumulative seismic moment of aftershocks is only $\sim 1\%$ of geodetic moment due to afterslip (Barbot et al., 2009). These observations imply that both the postseismic relaxation and aftershocks following the 2004 Parkfield mainshock were primarily driven by afterslip.

Recently, Kato (2007) conducted 3D numerical simulations to investigate the relationships among aftershocks, afterslip, effective normal stress s_{eff} (i.e., the normal stress minus the pore pressure), and frictional parameters a and b of the laboratory-derived rate-state dependent friction law (Dieterich, 1994). He showed that the radius of the aftershock area expands logarithmically with time since the mainshock, consistent with our observations. In addition, the rate of aftershock expansion is inversely proportional to the value of $A-B$ ($= (a-b)s_{eff}$) (Kato, 2007). His results further support the causal link between afterslip and aftershocks, and allow us to draw inference regarding the frictional parameters of the SAF from aftershock migration. As shown in Fig. 3, the aftershock area increases from ~ 32 km at 100 s to ~ 48 km at 10^5 s after the mainshock. Such expansion is roughly compatible with the migration of simulated aftershocks (Kato, 2007) in velocity strengthening region with the value of $A-B$ in the range of 0.2 to 0.5 MPa. Assuming an effective normal stress of 50 MPa, the corresponding value of $a-b$ is in the range of 0.004–0.01, which is close to the value of 0.007 obtained by geodetic inversion of Barbot et al. (2009), and higher than the value of 0.0001–0.002 obtained by Johnson et al. (2006).

2.5 Summary

In this study we focused on the spatio-temporal evolutions of early aftershocks in an unprecedented detail, based on the 11-fold increase of aftershock detections from the novel matched filter technique. The early aftershocks showed clear migration in along-strike and down-dip directions with the logarithmic time since the mainshock. So the aftershock expansion is most significant immediately after the mainshock, consistent with previous observations (e.g., Tajima and Kanamori, 1985) and recent numerical simulations (Kato, 2007). Our results suggest that systematic detection and analysis of early aftershocks not only provide important constraints on the mainshock rupture properties and aftershock migration patterns, but also shed new insights into postseismic deformation and frictional properties of the active fault zones.

3. Detection of triggered events on the SAF after the 2003 San Simeon earthquake

3.1 Previous observations

The 2003 M 6.5 San Simeon earthquake occurred in the central California coast on a reverse fault striking northwest and dipping northeast (Hardebeck et al., 2004). Nine months later, the 2004 M6.0 Parkfield earthquake occurred nearby on the SAF. The apparent spatial-temporal clustering between these two events may suggest a possible causal relationship between them. In

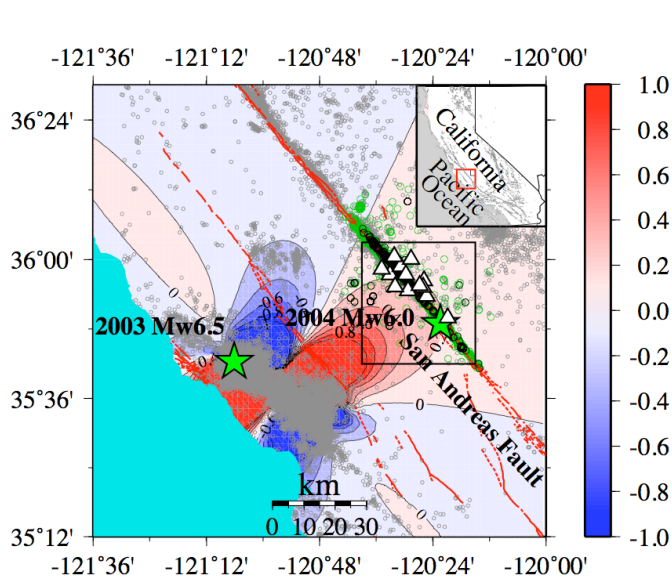


Figure 4. Map of the study region in central California. The active faults are marked as red lines, and the seismicity is shown as gray circle. The green stars show the epicentral locations of the 2003 Mw6.5 San Simeon and 2004 Mw6.0 Parkfield earthquakes. The small green circles are the 3647 template events around the Parkfield section of the San Andreas Fault, and the black circles denote the detected events after the San Simeon mainshock. The background color denotes the Coulomb stress changes on right-lateral faults produced by the San Simeon mainshock.

particular, Aron and Hardbeck (2009) found that the 2003 San Simeon earthquake has imparted a positive Coulomb stress increase (on the order of 0.5 MPa) on the Parkfield section of the SAF (Figure 4). This is also consistent with the observations of a right-lateral triggered slip on the SAF observed on the USGS creep meters, although the origin of the creep is likely shallow (Hardebeck et al., 2004). However, the cumulative number of earthquakes from the NCSN catalog along the Parkfield section of the SAF showed a minor decrease, rather than an increase of activity after the 2003 San Siemon mainshock, which is against the Coulomb stress calculation and the universal observation of seismicity increase following a moderate earthquake due to dynamic triggering (Hill and Prejean, 2007).

3.2 Detections of missing triggered earthquakes

Inspired by our previous studies on early aftershocks in Japan (Peng et al., 2007) and California (Peng et al., 2006; Peng and Zhao, 2009), we speculate that rigorous aftershock sequence from the San Simeon mainshock rupture region could mask the locally triggered microearthquakes on the SAF, resulting in an apparent decrease of seismicity immediately after the mainshock. To test such hypothesis, we apply the same matched filter technique to detect potential missing earthquakes on the SAF. We used the same ~3600 events as template, and scan through the continuous data 48 hours before and 30 hours after 2003 San Simeon earthquake recorded by the HRSN. The analysis procedure almost follow the same step as done before,

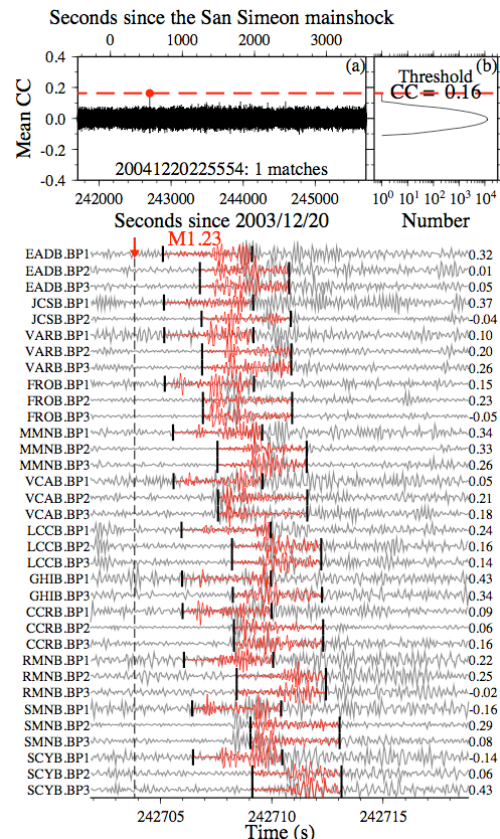


Figure 5. Example of a detected earthquake on the SAF about 500 s after the San Simeon earthquake. Other symbols and notations are the same as Figure 2.

except that we use 1 s before and 3 s after the P wave on the vertical component, and the same time window around the S wave on the two horizontal components, rather than the 2 s before and after the S wave on the three components (Peng and Zhao, 2009). The motivation behind such changes is that hopefully we can best capture the locally generated seismic signals by enforcing the S - P times.

Figure 5 shows an example of positive detection about 500 s after the San Simeon mainshock. Although the average CC value is just above the threshold of $9\times\text{MAD}$, the matching of the phases across multiple stations suggests that this is unlikely to be a random detection. The relative low CC value could be caused by the superposition of aftershock signals from the San Simeon mainshock

region as mentioned before, or the spatial separation between the template and the detect events.

Figure 6 summarizes the detection results. We found a total of 277 events 48 hours before and 30 hours after 2003 San Simeon earthquake, of which only 7 are listed in the NCSN catalog. The seismicity rate from the newly detected events shows a clear increase around Parkfield during the San Simeon mainshock. In comparison, swarm-like activity south of Gold Hill started about 2 days before and turned off immediately before the mainshock, which resulted in a decrease of seismicity rate. No detections are found further north in the creeping section of the SAF either before or after the mainshock.

Overall, our observations point to a positive increase of seismicity around the Parkfield section SAF immediately after the San Simeon earthquake, suggesting that the SAF near Parkfield was positively loaded by the San Simeon earthquake. This is also consistent with the aforementioned Coulomb stress calculation and triggered creep observations, although we cannot rule out the possibility of dynamic triggering at this stage.

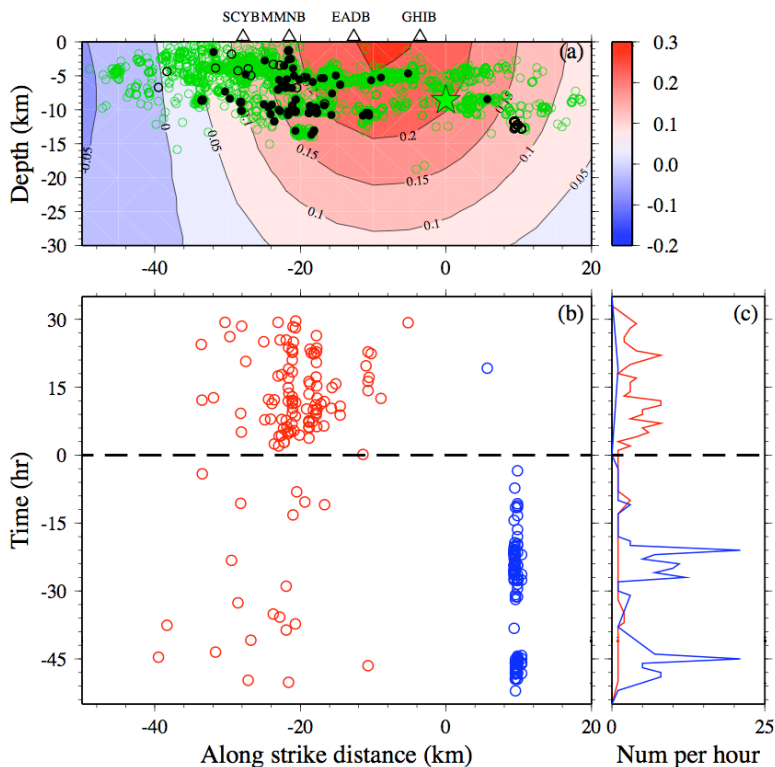


Figure 6. Spatial-temporal distributions of the detected events on the San Andreas Fault (SAF) around the San Simeon mainshock. (a) The green, open, and solid circles mark all the template events, events before and after the mainshock, respectively. The background color denotes the Coulomb stress changes resolved on the SAF. (b) Along-strike distances versus the time relative to the mainshock. The red and blue circles mark the events on the NW and SE of the epicenter of the 2004 Parkfield earthquake, respectively. (c) Number of earthquakes per hour for events on the NW (red) and SE of the epicenter, respectively.

4. Future work

Our results suggest that the matched filter technique is effective in detecting missing events immediately after nearby large earthquakes in Central California, and could lead to new insight in the mechanism of earthquake triggering, which is currently in heated debate (Felzer and Brodsky,

2006; Richards-Dinger et al., 2010). Currently we are applying the same technique to detect missing events in Southern California (Doran et al., 2010) and Japan (Enescu et al., 2010), and use the newly identified events to better quantify the underlying physical mechanism of earthquake triggering. In addition, we plan to examine the effect of the San Simeon earthquake in entire central California region, especially the creeping section of SAF, which was in the stress shadow from the Coulomb stress calculation. Applying the matched filter technique in this and other stress increase or shadow regions would allow us to better distinguish among different models and improve our understanding of earthquake interaction.

Bibliography

1. Publications

Peng, Z., and P. Zhao (2009), Migration of early aftershocks following the 2004 Parkfield earthquake, *Nature Geosci.*, 2, 877–881, doi: 10.1038/ngeo697.

Meng, X., Z. Peng and J. Hardebeck (2010), Detecting missing earthquakes on the Parkfield section of the San Andreas Fault following the 2003 Mw6.5 San Simeon earthquake, *Geophys. Res. Lett.*, in prep.

2. Conference abstracts

Peng, Z., B. Enescu, P. Zhao, and Sebastian Hainzl (2009), Detecting early aftershocks in California and Japan based on a matched filter technique, *Eos Trans. AGU*, 90(52), Fall Meet. Suppl., Abstract S54A-06.

Meng, X., Z. Peng and J. Hardebeck (2010), Detecting missing earthquakes on the Parkfield section of the San Andreas Fault following the 2003 Mw6.5 San Simeon earthquake, submitted to the 2010 annual AGU meeting, San Francisco.

Enescu, B., Z. Peng, K. Obara and T. Takeda (2010), Delay and migration of the 2008 Iwate-Miyagi early aftershocks, observed using high-resolution waveform data, submitted to the 2010 annual AGU meeting, San Francisco.

Doran, A., X. Meng, Z. Peng, and D. Kilb (2010), Dynamic triggering of earthquakes in the Salton Sea region of Southern California from large regional and teleseismic earthquakes, submitted to the 2010 annual AGU meeting, San Francisco.

References

- Aron, A., and J. L. Hardebeck (2009), Seismicity Rate Changes along the Central California Coast due to Coulomb Stress Changes from the 2003 M6.5 San Simeon and 2004 M6.0 Parkfield Earthquakes, *Bull. Seism. Soc. Am.*, 99, 2280-2292.
- Bakun, W. H., and A. G. Lindh (1985). The Parkfield, California, earthquake prediction experiment, *Science*, 229, 619–624.
- Bakun, W. H. et al. (2005), Implications for prediction and hazard assessment from the 2004 Parkfield earthquake, *Nature*, 437, 969–974, doi: 10.1038/nature04067.
- Barbot, S., Y. Fialko, and Y. Bock (2009), Postseismic deformation due to the Mw 6.0 2004 Parkfield earthquake: Stress-driven creep on a fault with spatially variable rate-and-state friction parameters, *J. Geophys. Res.*, 114, B07405, doi:10.1029/2008JB005748.
- Chatelain, J., R. K. Cardwell, and B. L. Isacks (1983), Expansion of the aftershock zone following the Vanuatu (New Hebrides) Earthquake on 15 July 1981, *Geophys. Res. Lett.*, 10(5), 385–388, doi:10.1029/GL010i005p00385.
- Dieterich, J. H. (1994), A constitutive law for rate of earthquake production and its application to earthquake clustering, *J. Geophys. Res.*, 99, 2601–2618.
- Doran, A., X. Meng, Z. Peng, and D. Kilb (2010), Dynamic triggering of earthquakes in the Salton Sea region of Southern California from large regional and teleseismic earthquakes, submitted to the 2010 annual AGU meeting, San Francisco.
- Enescu, B., Z. Peng, K. Obara and T. Takeda (2010), Delay and migration of the 2008 Iwate-Miyagi early aftershocks, observed using high-resolution waveform data, submitted to the 2010 annual AGU meeting, San Francisco.
- Felzer, K. R. and E. E. Brodsky (2006), Decay of aftershock density with distance indicates triggering by dynamic stress, *Nature*, 441, 735-738.
- Freed, A. M. (2007), Afterslip (and only afterslip) following the 2004 Parkfield, California, earthquake, *Geophys. Res. Lett.*, 34, L06312, doi:10.1029/2006GL029155.
- Hardebeck, J. L., J. Boatwright, D. Dreger, R. Goel, V. Graizer, K. Hudnut, C. Ji, L. Jones, J. Langbein, J. Lin, E. Roeloffs, R. Simpson, K. Stark, R. Stein, and J. C. Tinsley (2004), Preliminary Report on the 22 December 2003 M6.5 San Simeon, California, Earthquake, *Seism. Res. Lett.*, 75, 155-172.
- Harris, R. A. and J. R. Arrowsmith (2006), Introduction to the special issue on the 2004 Parkfield earthquake and the Parkfield earthquake prediction experiment, *Bull. Seismol. Soc. Am.*, 96(4B), S1-S10; doi: 10.1785/0120050831.
- Henry, C., and S. Das (2001), Aftershock zones of large shallow earthquakes: fault dimensions, aftershock area expansion and scaling relations, *Geophys. J. Int.*, 147, 272–293.
- Hickman, S., M. D. Zoback, and W. Ellsworth (2004), Introduction to special section: Preparing for the San Andreas Fault Observatory at Depth, *Geophys. Res. Lett.*, 31, L12S01, doi:10.1029/2004GL020688.
- Hill, D. P., and S. G. Prejean (2007). Dynamic triggering, in *Earthquake Seismology Treatise on Geophysics*, H. Kanamori (Editor), Elsevier, Amsterdam.
- Hsu, Y. J., M. Simons, J. P. Avouac, J. Galetzka, K. Sieh, M. Chlieh, D. Natawidjaja, L. Prawirodirdjo, and Y. Bock (2006), Frictional afterslip following the 2005 Nias-Simeulue earthquake, Sumatra, *Science*, 312, 1921-1926.
- Johnson, K. M., R. Burgmann, and K. Larson (2006), Frictional properties on the San Andreas fault near Parkfield, California inferred from models of afterslip following the 2004 earthquake, *Bull. Seism. Soc. Am.*, 96(4B), S321–S338.
- Kato, N. (2007), Expansion of aftershock areas caused by propagating post-seismic sliding, *Geophys. J. Int.*, 168, 797–808.

- Langbein, J., J. Murray, and H. A. Snyder (2006), Coseismic and initial postseismic deformation from the 2004 Parkfield, California, earthquake, observed by Global Positioning System, creepmeters, and borehole strainmeters, *Bull. Seism. Soc. Am.*, 96(4B), S304–S320.
- Meng, X., Z. Peng and J. Hardebeck (2010), Detecting missing earthquakes on the Parkfield section of the San Andreas Fault following the 2003 Mw6.5 San Simeon earthquake, submitted to the 2010 annual AGU meeting, San Francisco.
- Nur A., and J. R. Booker (1972), Aftershocks caused by pore fluid flow? *Science*, 175, 885–888.
- Richards-Dinger, K., R. S. Stein and S. Toda (2010), Decay of aftershock density with distance does not indicate triggering by dynamic stress, *Nature*, doi:10.1038/nature09402.
- Peng, Z., and P. Zhao (2009), Migration of early aftershocks following the 2004 Parkfield earthquake, *Nature Geosci.*, 2, 877–881, doi: 10.1038/ngeo697.
- Peng, Z., and Y. Ben-Zion (2006), Temporal changes of shallow seismic velocity around the Karadere-Duzce branch of the north Anatolian fault and strong ground motion, *Pure Appl. Geophys.*, 163, 567-599, doi: 10.1007/s00024-005-0034-6.
- Peng, Z., J. E. Vidale, and H. Houston (2006), Anomalous early aftershock decay rates of the 2004 M6 Parkfield earthquake, *Geophys. Res. Lett.*, 33, L17307, doi:10.1029/2006GL026744.
- Peng, Z., J. E. Vidale, M. Ishii, and A. Helmstetter (2007), Seismicity rate immediately before and after main shock rupture from high-frequency waveforms in Japan, *J. Geophys. Res.*, 112, B03306, doi:10.1029/2006JB004386.
- Perfettini, H. and J.-P. Avouac (2004), Postseismic relaxation driven by brittle creep: A possible mechanism to reconcile geodetic measurements and the decay rate of aftershocks, application to the Chi-Chi earthquake, Taiwan. *J. Geophys. Res.* 109, B02304, doi:10.1029/2003JB002488.
- Savage, J. C. and J. Langbein (2008), Postearthquake relaxation after the 2004 M6 Parkfield, California, earthquake and rate-and-state friction, *J. Geophys. Res.*, 113, B10407.
- Shelly, D. R., G. C. Beroza and S. Ide (2007a), Non-volcanic tremor and low-frequency earthquake swarms, *Nature*, 446, 305–307, doi:10.1038/nature05666.
- Shelly, D. R., G. C. Beroza, and S. Ide (2007b), Complex evolution of transient slip derived from precise tremor locations in western Shikoku, Japan, *Geochem. Geophys. Geosyst.*, 8, Q10014, doi:10.1029/2007GC001640.
- Sieh, K. (1978), Slip along the San Andreas fault associated with the great 1857 earthquake, *Bull. Seismol. Soc. Am.*, 68, 1421–1448.
- Tajima, F., and H. Kanamori (1985), Global survey of aftershock area expansion patterns, *Phys. Earth planet. Inter.*, 40, 77–134.
- Thurber, C. H. Zhang, F. Waldhauser, J. Hardebeck, A. Michael, and D. Eberhart-Phillips (2006), Three-dimensional compressional wavespeed model, earthquake relocations, and focal mechanisms for the Parkfield, California, region, *Bull. Seismol. Soc. Am.*, 96(4B), S38-S49, doi: 10.1785/0120050825.
- Waldhauser, F., W. L. Ellsworth, D. P. Schaff, and A. Cole (2004), Streaks, multiplets, and holes: High-resolution spatio-temporal behavior of Parkfield seismicity, *Geophys. Res. Lett.*, 31, L18608, doi : 10.1029/2004GL020649.